frontiers | Frontiers in Environmental Science

TYPE Original Research
PUBLISHED 01 February 2023
DOI 10.3389/fenvs.2023.1075842

OPEN ACCESS

EDITED BY
Sudhir Kumar Pandey,
Guru Ghasidas Vishwavidyalaya, India

REVIEWED BY
Haibo Li,
Northeastern University, China
Han Zhang,
Shenzhen University, China

*CORRESPONDENCE
Qing Zhao,
zhaoqing@iae.ac.cn

†These authors have contributed equally to this work and share last authorship

SPECIALTY SECTION
This article was submitted to Toxicology, Pollution and the Environment, a section of the journal Frontiers in Environmental Science

RECEIVED 21 October 2022
ACCEPTED 13 January 2023
PUBLISHED 01 February 2023

CITATION
Lei L, Zhang S, Lou W, Zhang X, Qin B, Zhao Q and Xing B (2023), Protection mechanism of N,N-dimethylformamide on stability of few-layer black phosphorus. *Front. Environ. Sci.* 11:1075842. doi: 10.3389/fenvs.2023.1075842

Protection mechanism of N,N-dimethylformamide on stability of few-layer black phosphorus

Lei Lei[1,2†], Siyu Zhang[1†], Wenhao Lou[1], Xuejiao Zhang[1], Bin Qin[1,2], Qing Zhao[1,3,4*] and Baoshan Xing[5]

[1]Key Laboratory of Pollution Ecology and Environmental Engineering, Institute of Applied Ecology, Chinese Academy of Sciences, Shenyang, China, [2]University of Chinese Academy of Sciences, Beijing, China, [3]Key Laboratory of Integrated Agro-Environmental Pollution Control and Management, Institute of Eco-Environmental and Soil Sciences, Guangdong Academy of Sciences, Guangzhou, China, [4]China National-Regional Joint Engineering Research Center for Soil Pollution Control and Remediation in South China, GuangZhou, China, [5]Stockbridge School of Agriculture, University of Massachusetts, Amherst, MA, United States

Few-layer black phosphorus (LBP) has been widely investigated for its unique optical and electronic properties. As degradation of LBP in ambient conditions largely limited its practical applications, numerous stabilization methods were developed. Understanding stabilization mechanism is essential to development of new protection technologies for LBP. Herein, protection mechanism of the most wildly used exfoliation solvent N,N-dimethylformamide (DMF) on LBP was investigated. DMF was found to accelerate color fading of LBP in aerobic water solution. Nevertheless, dissolvable phosphorus generated from degradation of LBP in the presence of DMF accounted for only 52%–57% of that generated in the absence of DMF. By measuring kinetics constants and activation energies of the degradation reactions, the protection mechanism of DMF was attributed to impede hydrolysis of phosphorus oxides. This was caused by occupation of oxidation sites on LBP by DMF through electrostatic interaction. Insoluble phosphorus oxides in addition to dissolvable phosphorus were observed in DMF exfoliated LBP aqueous solution, providing further evidence for hydrolysis impeding mechanism. This finding threw mechanism light on protection effects of DMF on LBP, providing new knowledge for development of effective stabilization technologies of LBP.

KEYWORDS

few-layer black phosphorus, N,N-dimethylformamide, electrostatic interaction, protection mechanism, hydrolysis of phosphorus oxides

Introduction

Few-layer black phosphorus (LBP), a new two-dimension material, displayed tunable direct band gap, excellent carrier mobility, high on/off ratios, and large specific surface and so on (Su et al., 2019). Desirable properties make LBP a promising candidate for high-performance electronic and optoelectronic device applications (Miao et al., 2019). LBP was prepared by exfoliating bulk black phosphorus (BP), which has a puckered honeycomb lattice structure with layers stacked together by van der Waals interaction (Li et al., 2022). The weak interlayer interaction allows bulk BP smoothly exfoliated into nanosheets, often resulting in dramatic changes to properties (Xue et al., 2017). Bulk BP is a stable allotrope of white and red phosphorus (Liu et al., 2016). However, LBP is very reactive to oxygen and water under ambient conditions (Abellan et al., 2017), resulting in compositional and physical changes and

consequently considerable degradation in the electronic and optical properties (Abellan et al., 2017). Degradation of LBP is thickness-dependent (Gamage et al., 2017). For example, LBP less than 10 nm thickness degraded in days (Castellanos-Gomez et al., 2014), whereas single- and few-layer LBP may degraded within hours (Island et al., 2015). Therefore, different stabilization techniques were developed to overcome the challenges of intrinsic instability of LBP and to realize better applications.

Stabilization techniques of LBP included chemical protection methods (covalent functionalization (Hu H. et al., 2018) and non-covalent functionalization (Abellán et al., 2016)), physical methods (capping layers (van Druenen, 2020) and polymer-based protection (Li et al., 2016)) and solvent-based stabilization methods (Hanlon et al., 2015). Chemical protection methods introduced organic compound ligands, and then potentially caused chemical pollution (Jia et al., 2019). Physical protection methods not only require demanding operation techniques and complicated environmental conditions, but also make LBP difficult to interact with metal contacts or chemical reagents (Yan et al., 2020). In contrast, the solvent stabilization is a promising protection method for LBP as solvent is easily removed (Yan et al., 2018), and not influences optoelectronic properties of LBP (Kang et al., 2015).

Compared with micromechanical exfoliation (Suryawanshi et al., 2016), adhesive tape (Lewis et al., 2017), and chemical vapor deposition (Smith et al., 2016), exfoliation of layered materials by liquid-phase exfoliation (LPE) appears to be facile and potentially scalable for practical manufacture (Zhang et al., 2017). Selecting a suitable LPE system is a key factor for exfoliation and dispersion of LBP. LPE developed for LBP included pure (Sresht et al., 2015) and mixed (Ge et al., 2019) organic solvents, ionic liquids (Zhao et al., 2015), polymer solutions (Shen et al., 2021), and even pure water (Zhang et al., 2019).

LPE in pure organic solvents was able to protect LBP from reacting with water or oxygen by forming solvation shells (Hanlon et al., 2015). LBP exfoliation becomes easier in an order of N,N-dimethylformamide (DMF) > N-methyl-2-pyrrolidone (NMP) > dimethyl sulfoxide > isopropanol (Sresht et al., 2015). Among pure organic solvents, DMF is the most commonly used for exfoliating LBP and promotes stabilization of LBP. DMF-coating LBP degraded only 30% after 13 d of ambient exposure (Liu et al., 2019), while bare LBP of similar thickness almost completely degraded within 10 d of ambient exposure (Ryder et al., 2016). So far, mechanism of DMF protecting LBP from degradation was not known yet.

Most previous studies were focused on degradation of LBP in pure organic solvent (Hanlon et al., 2015). However, in practical application, LBP was usually used in ambient environment with presence of water and air (Matthews et al., 2018). For examples, LBP exfoliated by NMP was used as adsorbent to remove methylene blue from aqueous solution (Wang et al., 2020), or used as humidity sensor in ambient environment (Late, 2016). LBP exfoliated by DMF exhibited perfect photothermal effect, and was used to capture bacterial cells in water for disinfection (Deng et al., 2022). The role of organic solvent molecules on stabilization of LBP used in water matrix was largely not known yet.

In this study, protection mechanism of DMF on LBP in water was investigated. Results showed that electrostatic interaction was the primary interaction force between DMF and LBP. DMF occupied oxidation sites on LBP, promoted reactivity of LBP with O_2, but hindered the hydrolysis of phosphorus oxide. Previous stabilization methods of LBP usually worked by protecting lone-pair electrons of LBP and hindered reactions with O_2 (Peng et al., 2020). This study revealed a new protection mechanism of DMF by occupying oxidation sites on LBP, which casted new light on the development of effective stabilization technologies of LBP.

Materials and methods

Materials

Crystalline BP (purity >99.998%) was obtained from Xianfeng Nano Co., Ltd. (Nanjing, China). DMF and D_2O (purity 99.5%) were from Beijing J&K Scientific Ltd. Ultrapure water was prepared with a Millipore-Milli Q system.

Experimental methods

Preparation of LBP Nanoflakes in Water. LBP was prepared by exfoliating bulk BP crystals in anaerobic water. To improve exfoliation efficiency, the bulk BP was ground in an agate mortar to obtain large BP flakes, and then transferred into a 250 ml anaerobic glass bottle filled with anaerobic ultrapure water. The procedures were performed in an anaerobic glovebox to prevent LBP from contacting with oxygen. Anaerobic water was obtained by pre-heating ultrapure water to 70°C and purged with high-purity N_2 for over 120 min to exclude dissolved O_2, sealed and moved into glovebox immediately. The anaerobic bottle containing BP flakes was sealed tightly and sonicated for 21 h with an immersion probe at 360 W (1800–99, Biosafer). During ultrasonication, the bottle was placed in an ice-bath to keep temperatures below 15°C. After ultrasonication, the suspension was centrifuged at 88 g for 30 min to remove unexfoliated large BP flakes. Subsequently, supernatants were centrifuged at 1800 g for 30 min to remove precipitates. LBP nanoflakes in the supernatants (H_2O-LBP) were used for further experiments.

Preparation of LBP Nanoflakes in DMF. All procedures were the same as above except that ultrapure water was changed into DMF. After the second centrifugation, the supernatants were further centrifuged at 10,000 rpm for 30 min to collect DMF exfoliated LBP (DMF-LBP) in precipitates. The precipitates were re-dissolved in anaerobic ultrapure water for further experiments.

Degradation Experiments. Degradation experiments were performed in pH 7–10 $NaHCO_3/Na_2CO_3$ buffer solutions. Cationic strength was adjusted to 2 mmol/L. All containers were wrapped with aluminum foils and placed in the dark to prevent light. The solutions were injected with pure O_2 every day to maintain a saturation status of O_2. Degradation kinetics experiments were performed at 15°C ± 1°C, 25°C ± 1°C, 37°C ± 1°C, 45°C ± 1°C or 55°C ± 1°C.

Degradation kinetics curves were fitted by apparent first-order kinetics equation (Eq. 1):

$$\ln(C_t) = \ln(C_0) - kt \quad (1)$$

where C_0 and C_t were concentrations of LBP at initial and at time t, respectively. k was degradation rate constant; C_0 was obtained by measuring total dissolvable phosphorus (TDP) after all LBP was degraded (TDP_∞) or UV absorbance of LBP at 255 nm before degradation (A_0); C_t was obtained from Eq. 2:

$$C_t = TDP_\infty - TDP_t = A_t \quad (2)$$

where TDP_t was TDP at time t; A_t was UV absorbance of LBP at 255 nm at time t. Accordingly, Eq. 1 was transformed into Eqs. 3, 4, and k was slope of the kinetics curve obtained by plotting ln (TDP_∞ - TDP_t) or ln (A_t) against t:

$$\ln(TDP_\infty - TDP_t) = \ln(TDP_\infty) - kt \quad (3)$$

$$\ln(A_t) = \ln(A_0) - kt \quad (4)$$

Activation energy (E_a, kJ/mol) provided information of critical energy for starting of degradation reaction (Yao et al., 2008). The relationship between E_a and k follows Arrhenius equation (Brachi et al., 2021) (Eq. 5), and E_a/R is the slope of the curve obtained by plotting log$k$ against 1/T (Oza et al., 2014).

$$k = A\exp(-E_a/RT) \quad (5)$$

where A was a pre-exponential factor, T was the temperature K), and R was the gas constant (8.314 J mol^{-1} K^{-1}). Each experiment was repeated in triplicate. Data reported were average values for the triplicate experiments.

Electrochemical Experiments. Interaction sites of DMF with LBP was probed by electrochemical experiments performed with CHI660E electrochemical working station (Shanghai Chenhua Instrument, China). A three-electrode system was employed. The reference and the counter electrodes were Ag/AgCl and Pt wire electrodes, respectively. Electrolyte was N_2-saturated 0.5 M H_2SO_4 (pH = 1) solution, respectively. H_2O-LBP and DMF-LBP were used as working electrodes. Linear sweep voltammetry (LSV) was used to evaluate hydrogen evolution reaction (HER) performance of the working electrodes. Scan rate was 5 mV/s. Applied potentials were shown as reversible hydrogen electrode (RHE) potentials ($E_{vs\ RHE}$) based on the Nernst function (Eq. (6)) (Benck et al., 2014).

$$E_{vs\,RHE} = E_{vs\,Ag-AgCl} + E^\circ_{(Ag/AgCl)} + 0.059 \times pH \quad (6)$$

where $E_{vs\ Ag\text{-}AgCl}$ was the experimentally measured potential V) and $E^\circ_{(Ag/Ag/Cl)}$ was the standard potential (0.199 V) at 25°C.

Characterization and Analysis. Electrophoretic mobility (EPM) and hydrodynamic diameter were measured by time-resolved dynamic light scattering (Nano-ZS, Malvern) operated at 173° scattering angle. Atomic force microscope (AFM, Agilent 5,100) was used to characterize thickness of LBP. Functional groups on the surface of LBP were characterized by Fourier transform infrared spectroscopy (FTIR, Nicolet IS 10). LBP solutions were freeze-dried, and then mixed with KBr powder for FTIR analysis. The content of phosphorus oxides (P_xO_y) for LBP was determined by X-ray photoelectron spectroscopy (XPS, ESCALAB250, Thermo VG). LBP nanoflakes were washed with ultrapure water to remove residual salts before XPS measurements. The aliphatic C 1s peak (284.6 eV) was used as an internal standard to correct the peak shifts (Barrère et al., 2003). The relative atomic concentrations were determined according to integrated peak areas of P 2p and O 1s peaks based on Lorentzian-Gaussian functions and using the Scofield sensitivity coefficients (Barrère et al., 2003). The peaks were fitting using XPSPEAK software.

Light absorbance of LBP was recorded by UV-vis spectrophotometer (Shimadzu UV-2700). TDP was quantified by inductively coupled plasma optical emission spectrometry (Agilent 5,100). Dissolved phosphorous species were identified by ^{31}P nuclear magnetic resonance spectroscopy (^{31}P NMR, AVANCE600, Bruker). After degradation for 4 months, 40 ml H_2O-LBP and DMF-LBP (5.6 mg/L) were freeze-dried, and re-dissolved with 1 ml D_2O for the ^{31}P NMR analysis.

Results and disscussion

Characterization of LBP

AFM images indicated that thickness and lateral sizes of H_2O-LBP and DMF-LBP were close (Supplementary Figure S1). Based on statistical results from 100 pieces, average thicknesses of H_2O-LBP and DMF-LBP were 4.02 ± 3.05 and 4.49 ± 3.26 nm (Figure 1A), and average lateral sizes were 311.6 ± 12.7 and 289.2 ± 9.1 nm (Figure 1B), respectively. Average hydrodynamic diameter values of H_2O-LBP and DMF-LBP were 267.7 ± 17.3 and 260.8 ± 11.2 nm at pH 7 (Figure 1C). Accordingly, the two types of LBP had similar thicknesses, hydrodynamic sizes and plane surface areas.

FTIR spectra (Figure 1D) showed presence of chemically reactive functional groups on both LBP, including HO-P=O (1,637 cm^{-1}), P=O (1,379 cm^{-1}), P-OH (1,078 cm^{-1}), P-O-P (1,148 cm^{-1}) (Druenen et al., 2019; Guo et al., 2021). Compared with H_2O-LBP, a new peak at 798 cm^{-1}, corresponding to CH_2 rocking (Tiouitchi et al., 2019), was observed for DMF-LBP. The FTIR results indicated that DMF was adsorbed on the surface of LBP. XPS spectra (Supplementary Figures S1E, F) showed two peaks at 130.0 and 129.0 eV assigning to binding energies of $2p_{1/2}$ and $2p_{3/2}$, respectively, corresponding to P-P bonds of LBP. A small peak at 131.6 eV belonged to P_xO_y, which was mainly derived from oxidation of LBP during ultrasonication or from irreducible water (Zhang et al., 2019). Relative intensities of P_xO_y to total P of H_2O-LBP and DMF-LBP were 7.10% and 10.3% (Supplementary Table S1), respectively. Accordingly, oxidation degree of DMF-LBP was a bit higher than that of H_2O-LBP.

Due to slight oxidation during ultrasonication, LBP carried net negative charges (Figure 1C). Oxidation functional groups of LBP contained P=O, P-OH and P-O-P components (Supplementary Figures S1G, H). Compared with P=O and P-O-P, P-OH contributed more to negative charges (García-Sancho et al., 2018). Both oxidation degree (10.3%) and percentage of P–OH (79%) of DMF-LBP were higher than that of H_2O-LBP (P_xO_y: 7.10%; P-OH: 32.3%) (Supplementary Table S1). Theoretically, DMF-LBP was inferred to carry more net negative charges than H_2O-LBP. However, EPM of DMF-LBP (−2.48 ± 0.12 μm cm Vs^{-1}) was higher than that of H_2O-LBP (−3.30 ± 0.13 μm cm Vs^{-1}) in pH 7.0 aqueous solution (Figure 1C).

Interaction mechanism between DMF and LBP

The EPM values of H_2O-LBP in 0.5%–10% DMF aqueous solutions were measured at pH 7.0. The values increased from −3.30 ± 0.1 to −2.41 ~ −2.74 μm cm Vs^{-1} with increases of DMF (Supplementary Figure S1I). Previous studies showed that the EPM was usually used as an index of the magnitude of electrostatic interaction of the solutes (White et al., 2007; Pedersen et al., 2018). The evolution of EPM meant that the electrostatic interaction between DMF and H_2O-LBP became weaker with increases of DMF. Generally, large EPM absolute value indicates better dispersion of the solute (Li et al., 2017). The EPM value of H_2O-LBP in 0.5% DMF aqueous solution was higher than that in 1% DMF aqueous solution (Supplementary Figure S1I), suggesting that the dispersion of H_2O-LBP should be better in 1% DMF aqueous solution than in 0.5% DMF aqueous solution. On

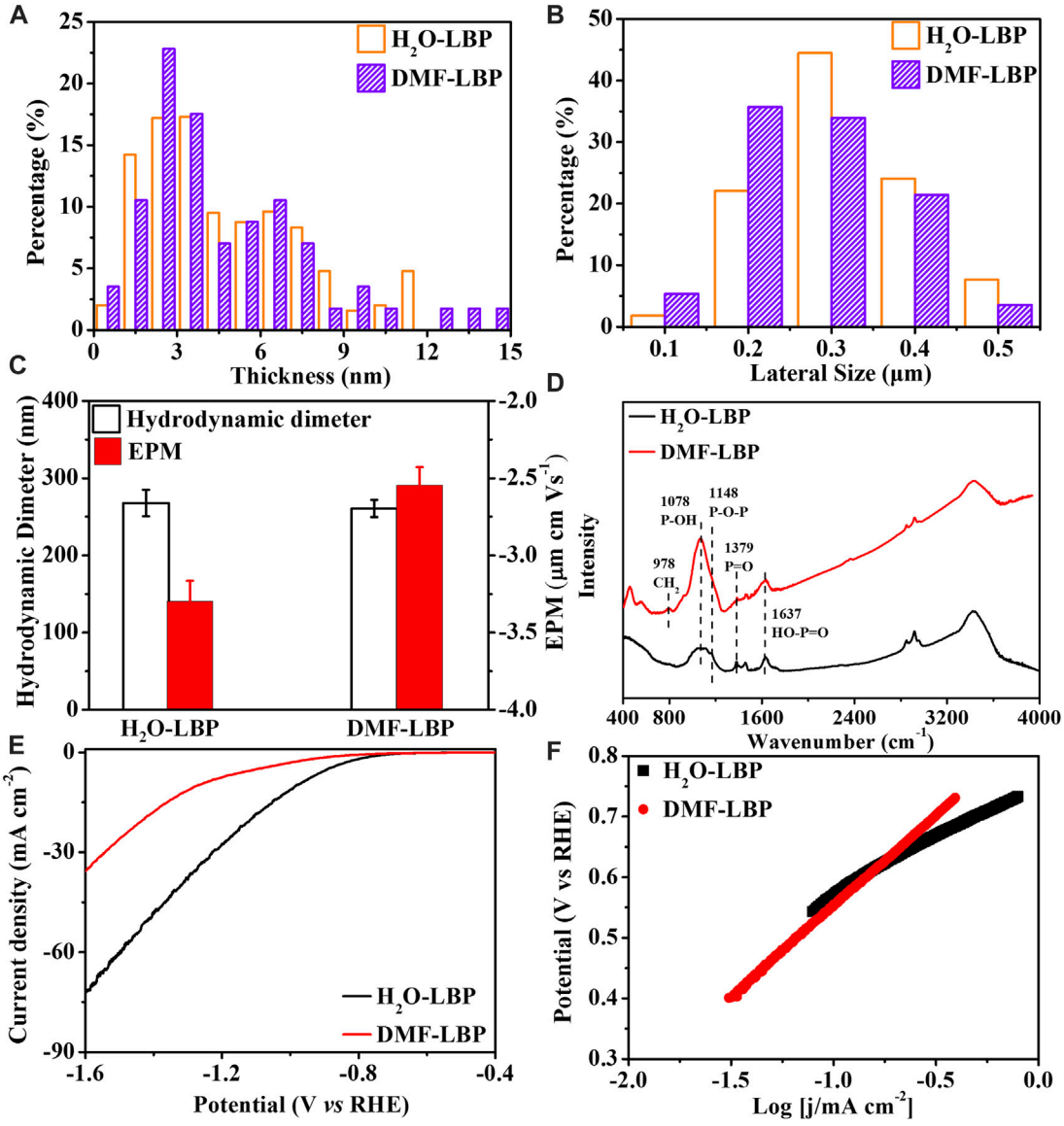

FIGURE 1
Characterizations of LBP. Thicknesses **(A)** and lateral sizes **(B)** of two types of LBP nanoflakes **(C)** Hydrodynamic diameters and EPM of two types of LBP at pH 7 **(D)** FTIR spectra of two types of LBP; Polarization curves **(E)** and Tafel plots **(F)** of both LBP in N_2-saturated 0.5 mol L^{-1} H_2SO_4 solution.

the contrary, the hydrodynamic diameter of H_2O-LBP indicated that dispersion in 0.5% DMF aqueous solution was not as good as that in 1% DMF aqueous solution (Supplementary Figure S1I). According to previous study, high concentration of DMF could transform graphene oxide nanomembranes to nanoscrolls (Tang et al., 2018). Similarly, DMF promoted the curling of LBP nanosheets, resulting in the oxidation functional groups originally formed on the LBP surface being wrapped. With increases of DMF, more oxidation functional groups were wrapped due to curling. As EPM was mainly derived from negative charges carried by the oxidation functional groups, it is not surprised that EPM was increased with increases of DMF.

Electrostatic interaction Between LBP and DMF was further evidenced by the effect of DMF on electrocatalytic activities for HER of LBP. Electrocatalytic activities for HER of H_2O-LBP and DMF-LBP were investigated in N_2-saturated 0.5 M H_2SO_4 solution according to polarization curves (Figure 1E). Compared with DMF-LBP (−849 mV vs. RHE), H_2O-LBP exhibited a higher onset potential of −749 mV (vs. RHE), implying H_2O-LBP had higher electrocatalytic activity for HER. H_2O-LBP produced current density of 10 and 30 mA cm^{-2} at potentials of −0.98 and −1.23 V, while DMF-LBP needed higher negative potentials (−1.27 V for 10 mA cm^{-2}; −1.54 V for 30 mA cm^{-2}). Therefore, DMF weaken the electrocatalytic activity for HER of LBP.

HER involved three possible reaction steps based on two mechanisms: Volmer-Heyrovsky and Volmer-Tafel (Kwak et al., 2016).

$$\text{Volmer step: } H^+ + e^- \rightarrow H_{ad} \quad (7)$$

$$\text{Heyrovsky step: } H^+ + H_{ad} + e^- \rightarrow H_2 \quad (8)$$

$$\text{Tafel step: } 2H_{ad} \rightarrow H_2 \quad (9)$$

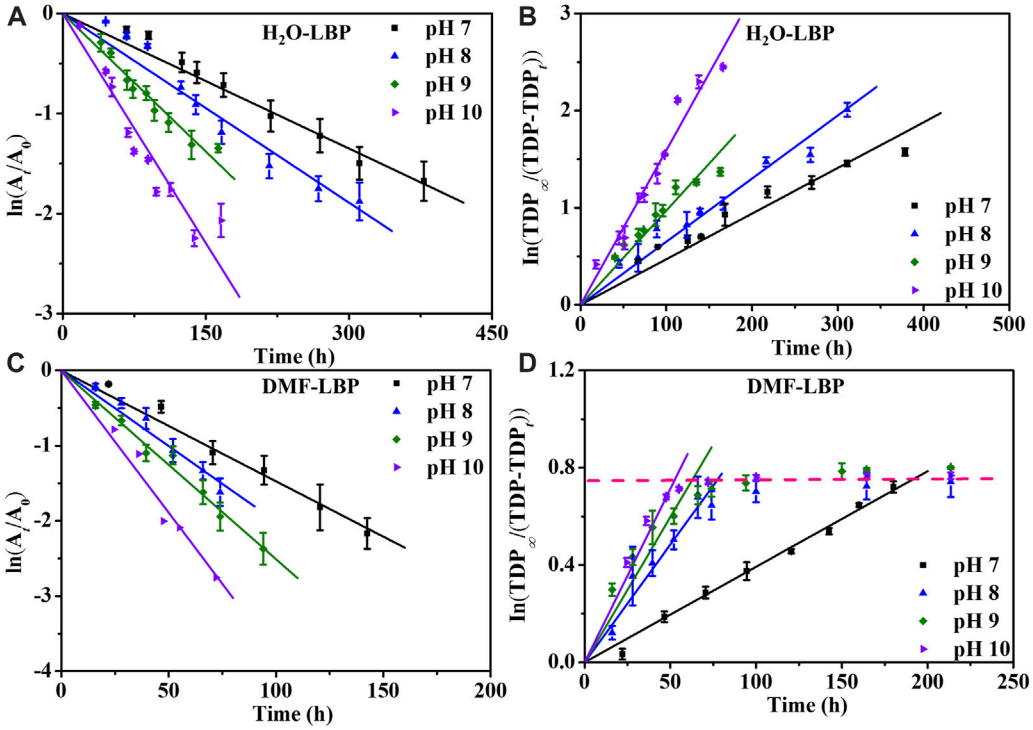

FIGURE 2
Degradation kinetics curves of LBP based on UV absorbance **(A, C)** and based on TDP **(B, D)** at different pH under 37°C ± 1°C. A_0 and A_t: UV absorbance at time 0 and *t*; TDP_∞: total concentration of P in LBP; TDP_t: TDP at time *t*.

These reactions corresponded to three possible rate determining steps: Volmer, Heyrovsky and Tafel (Kwak et al., 2016). Tafel plots was an important diagnostic tool delineating rate determining steps, providing insights into reaction mechanism of electrocatalyst (Murthy et al., 2018).

$$\eta = \rho \log j + a \quad (10)$$

where η is overpotential, j is current density, a is exchange current density, ρ is Tafel slope. ρ value was expected to be ca. 120 (for Volmer), 40 (for Heyrovsky) or 30 (Tafel) mV dec^{-1} (Chen et al., 2021) for different rate-determining steps of HER.

As shown in Figure 1F, ρ value of H_2O-LBP and DMF-LBP were 186 mV dec^{-1} and 299 mV dec^{-1}, respectively. Therefore, the Volmer HER mechanism representing weak adsorption of protons on the surface of catalysts (Kunimatsu et al., 2005) was rate-determining step for both the two LBP. The ρ value of DMF-LBP was higher than that of H_2O-LBP, meaning DMF hindered sorption of protons on LBP. Previous studies showed that negative charged P-site on LBP was the active sites to complete HER (Li and Wang, 2020). This further confirmed that DMF occupied negative charged P-sites originating form oxidation sties on LBP through electrostatic interaction.

Influence of DMF on hydrolysis of LBP

The color fading process of LBP was the slowest at pH 7, and the fastest at pH 10 (Supplementary Figure S2). For both LBP, increases of TDP and decreases of UV absorbance with time was the slowest at pH 7 and the fastest at pH 10 (Supplementary Figure S3). This was consistent with our previous studies that the degradation of LBP was pH-dependent (Zhang et al., 2019). Compared with H_2O-LBP, the color became invisible within 5 d at pH 7–8. It seemed that DMF-LBP degraded faster than H_2O-LBP.

Kinetics fitting results (Figure 2; Supplementary Table S1) showed that the apparent first-order degradation rate constants increased from pH 7 to 10 (R^2 = 0.92–0.97) for both LBP, attributed to the increases of HO^- (Zhang et al., 2019). The reaction rate constant (k_r) calculated based on the UV absorbance (Figure 2A) were close to that calculated based on TDP (k_f) (Figure 2B) for H_2O-LBP nanoflakes at pH 7–10. But k_r was almost 0.97 ~ 2.74 folds higher than k_f for DMF-LBP ((Figures 2C,D; Supplementary Table S2). This meant that the degradation of DMF-LBP indicated by increases of TDP contributed to only 26.7–50.8% of the total loss of DMF-LBP represented by decreases of UV absorbance. The rate gap ($k_r > k_f$) has been observed in the degradation of H_2O-LBP at pH 4 and 5, and was mainly attributed to deposition/aggregation (Zhang et al., 2019). However, hydrodynamic diameters measured during degradation of both LBP showed no significant changes (Supplementary Figure S4), indicating that deposition/aggregation was not the primary reason causing the rate gap for DMF-LBP.

The degradation of LBP to form dissolvable phosphorus proceeded through two steps, including generation of oxidation functional groups on surface caused mainly by O_2, and subsequent hydrolysis of the oxidation functional groups induced by H_2O (Zhou et al., 2016). Either the oxidation or the hydrolysis procedure can cause changes to UV absorbance, while only both the oxidation and hydrolysis reactions occurred can lead to increases of TDP. For H_2O-LBP, k_f was close to k_r, indicating that almost all oxidized

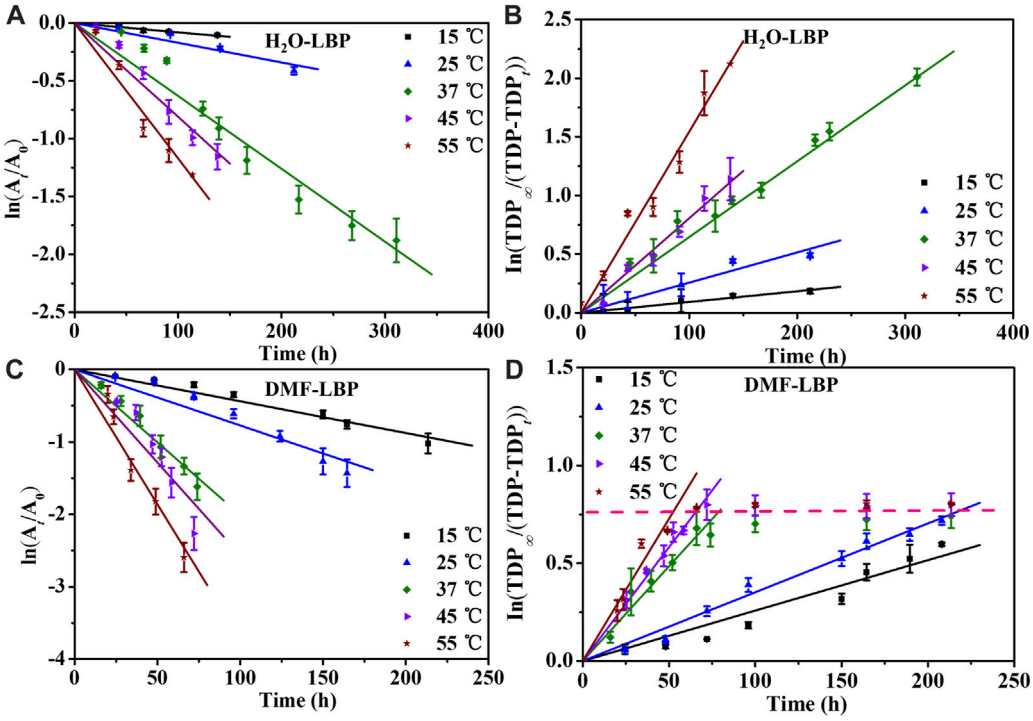

FIGURE 3
Degradation kinetics curves of LBP based on UV absorbance **(A, C)** and based on TDP **(B, D)** at pH 8 under different temperatures. A_0 and A_t: UV absorbance at time 0 and *t*; TDP_∞: total concentration of P in LBP; TDP_t: TDP at time *t*.

phosphorus underwent hydrolysis to form dissolvable phosphorus. For DMF-LBP, k_r was higher than k_f though the oxidation degree was high, implying that the hydrolysis reactions of phosphorus lagged behind oxidation of phosphorus (Supplementary Table S2).

According to XPS analysis, after 60% decreases of UV absorbance, the relative intensity of oxidized P in DMF-LBP was 78.2%, increasing by 6.56 folds compared with pristine DMF-LBP (Supplementary Figure S5; Supplementary Table S3). For H_2O-LBP, the increases were 1.23 folds. TDP of DMF-LBP remained 2.89–3.06 mg/L after 164, 150, 72 h at pH 8, 9 and 10 (Figure 2D; Supplementary Figure S3D), while that of H_2O-LBP continuously increased to 5.6 mg/L. This meant that only 52%–57% of the phosphorus oxides hydrolyzed into dissolvable phosphorus in the case of DMF-LBP, while all phosphorus oxides hydrolyzed in H_2O-LBP system. This result further indicated that the hydrolysis reactions of DMF-LBP were weakened compared with H_2O-LBP.

According to ^{31}P NMR spectrograms (Supplementary Figure S6), the total abundance of dissolvable degradation products of DMF-LBP was 53% of that of H_2O-LBP after degrading for 4 months. This ratio was close to that of TDP relative to TDP_∞ for DMF-LBP. The XPS results (Supplementary Figure S1, S5; Supplementary Tables S1, 3) showed the relative abundance of residual oxygen-containing functional groups were unchanged during degradation of H_2O-LBP, while decreases of P-OH and increases of P-O-P and P=O were observed for DMF-LBP after degradation. As P-OH was mainly generated by hydrolysis of P-O-P (Wu et al., 2018), this meant that P=O and P-O-P on the surface of DMF-LBP were relatively stable. As DMF impeded the hydrolysis reactions, more P_xO_y was remained on surface of DMF-LBP in comparison with H_2O-LBP, on which P_xO_y fast hydrolyzed to soluble phosphorus oxides. Therefore, the oxidation degree of H_2O-LBP was observed to be higher than that of DMF-LBP (Supplementary Figures S1E, F; Supplementary Table S1).

Influence of DMF on oxidation of LBP

The k_r values of DMF-LBP were 1.47–2.29 folds higher than that of H_2O-LBP at pH 7–10 (Supplementary Table S2). Therefore, oxidation reactions of LBP to form oxidation functional groups were inferred to be accelerated by DMF, though hydrolysis reactions were impeded by DMF. To prove this, E_a of oxidation reaction between O_2 and LBP was investigated. Kinetic fitting results (Figure 3; Supplementary Figure S7; Supplementary Table S4) showed that the apparent first-order degradation rate constant increased from 15°C to 55°C at pH 8 and 9 (R^2 = 0.92–0.97). Taking pH 8 as an example, the k_r values increased by 13.94 and 7.49 folds for H_2O-LBP and DMF-LBP from 15°C to 55°C (Figures 3A,C; Supplementary Table S4); k_f values increased by 14.63 and 4.66 folds for H_2O-LBP and DMF-LBP from 15°C to 55°C (Figures 3B,D; Supplementary Table S4).

E_a values of H_2O-LBP calculated based on k_r were 55.66 and 47.78 kJ/mol at pH 8 and 9, comparable with that obtained based on k_f (pH 8: 55.55 kJ/mol; pH 9: 50.22 kJ/mol) (Figures 4A,B). For DMF-LBP, E_a values calculated based on k_r were 43.58 and 39.64 kJ/mol at pH 8 and 9, and were 6.31 and 4.06 kJ/mol higher than that obtained based on k_f (pH 8: 37.26 kJ/mol; pH 9: 35.58 kJ/mol). According to above discussion, the differences between k_r and k_f were mainly attributed to influence of DMF on hydrolysis of phosphorus

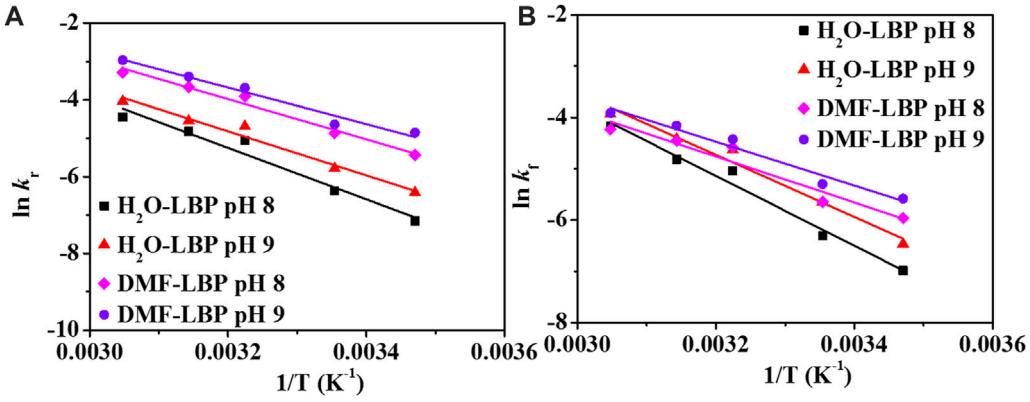

FIGURE 4
Plots lnk_r **(A)** and lnk_f **(B)** vs. 1/T at pH 8 and 9. k_r: reaction rate constant calculated based on the UV absorbance; k_f: reaction rate constant calculated based on TDP.

oxides. The different E_a values obtained for DMF-LBP indicated that energy barriers of hydrolysis reactions increased by DMF, resulting in accumulation of phosphorus oxides on the surface of LBP. By comparing E_a values of DMF-LBP and H_2O-LBP, energy barriers for oxidation were changed due to presence of DMF. Taking pH 8 as an example, E_a values of DMF-LBP calculated based on the k_f were 18.29 kJ/mol lower than that of H_2O-LBP due to presence of DMF. This meant that DMF lowered the energy barrier of the reaction between oxygen and LBP. This was consistent with the degradation kinetics results (Figure 2; Figure 3) that oxidation degree of DMF-LBP was higher than that of H_2O-LBP after the same experimental period.

As reported previously, in DMF solution, stability of LBP was improved due to the formation of solvation shell as a barrier to prevent LBP from reacting with water or oxygen in the air (Hu C.-X. et al., 2018; van Druenen, 2020). But the degradation of DMF exfoliated LBP was observed to accelerate due to increases of relative humidity when directly exposed to air (Yasaei et al., 2015), indicating that DMF may play different roles on degradation of LBP in the presence of water compared with pure DFM solution. In this study, DMF was found to play a double-edged role on degradation of LBP in water. On one hand, DMF occupied oxidation sites on LBP through electrostatic interaction, and promoted reactivity of LBP with O_2. On the other hand, DMF hindered the hydrolysis of phosphorus oxide formed on surface of LBP. This study indicated a protection mechanism of DMF in water different from that reported in previous studies focused on degradation in pure organic solvent.

Conclusion

In summary, we revealed the influence mechanism of DMF on degradation and of LBP. The results showed the electrostatic interaction was responsible for sorption of DMF on LBP. DMF exhibited as a double-edged sword in the degradation of LBP. In one aspect, DMF-LBP showed lower energy barrier for reaction with O_2 than H_2O-LBP, meaning DMF promoted the oxidation of LBP. In the other aspect, the hydrolysis reactions of phosphorus were impeded by DMF. This finding unveiled the protection mechanism of DMF on LBP, which facilitated the development of effective stabilization of LBP.

Data availability statement

The original contributions presented in the study are included in the article/Supplementary Material, further inquiries can be directed to the corresponding author.

Author contributions

LL, SZ, and QZ conceived and designed the experiments. LL, WL, and BQ performed experiments. SZ, XZ, BX, and QZ supervised the research and contributed to the manuscript writing. All authors read and approved the final manuscript.

Funding

This work is supported by the National Natural Science Foundation of China (42022056, 42192574, 22176196, 21976186, 42077394), GDAS' Project of Science and Technology Development (2022GDASZH-2022010105, 2020GDASYL-20200101002).

Acknowledgments

The authors also acknowledge Liaoning Province Natural Science Foundation (2020-YQ-10), Revitalize Liaoning Talents Program (XLYC2007124, XLYC1907136, XLYC1907118).

Conflict of interest

The authors declare that the research was conducted in the absence of any commercial or financial relationships that could be construed as a potential conflict of interest.

The reviewer (HL) is currently organizing a Research Topic with the author (SZ).

Publisher's note

Supplementary material

The Supplementary Material for this article can be found online at: https://www.frontiersin.org/articles/10.3389/fenvs.2023.1075842/full#supplementary-material

References

Abellán, G., Lloret, V., Mundloch, U., Marcia, M., Neiss, C., Görling, A., et al. (2016). Noncovalent functionalization of black phosphorus. *Angew. Chem.* 128 (47), 14777–14782. doi:10.1002/ange.201604784

Abellan, G., Wild, S., Lloret, V., Scheuschner, N., Gillen, R., Mundloch, U., et al. (2017). Fundamental insights into the degradation and stabilization of thin layer black phosphorus. *J. Am. Chem. Soc.* 139 (30), 10432–10440. doi:10.1021/jacs.7b04971

Barrère, F., Lebugle, A., Van Blitterswijk, C. A., De Groot, K., Layrolle, P., and Rey, C. (2003). Calcium phosphate interactions with titanium oxide and alumina substrates: An XPS study. *J. Mater. Sci. Mater. Med.* 14 (5), 419–425. doi:10.1023/a:1023210817683

Benck, J., Hellstern, T., Kibsgaard, J., Chakthranont, P., and Jaramillo, T. (2014). Catalyzing the hydrogen evolution reaction (HER) with molybdenum sulfide nanomaterials. *ACS Catal.* 4 (11), 3957–3971. doi:10.1021/cs500923c

Brachi, P., Santes, V., and Torres-Garcia, E. (2021). Pyrolytic degradation of spent coffee ground: A thermokinetic analysis through the dependence of activation energy on conversion and temperature. *Fuel* 302, 120995. doi:10.1016/j.fuel.2021.120995

Castellanos-Gomez, A., Vicarelli, L., Prada, E., Island, J. O., Narasimha-Acharya, K. L., Blanter, S. I., et al. (2014). Isolation and characterization of few-layer black phosphorus. *2D Mater.* 1 (2), 025001. doi:10.1088/2053-1583/1/2/025001

Chen, D., Tong, Z., Xiong, Z., Zhang, X., Zhao, Q., and Zhang, S. (2021). Environmental stability and cytotoxicity of layered black phosphorus modified with Polyvinylpyrrolidone and Zeolitic Imidazolate Framework-67. *Sci. Total Environ.* 790, 148105. doi:10.1016/j.scitotenv.2021.148105

Deng, S., Wang, D., Xiong, Z., Zhang, S., Li, D., Zeng, J., et al. (2022). Thermo-responsive polymer–black phosphorus nanocomposites for NIR-triggered bacterial capture and elimination. *Environ. Sci. Nano* 9 (4), 1330–1340. doi:10.1039/d1en00658d

Druenen, M., Davitt, F., Collins, T., Glynn, C., O'Dwyer, C., Holmes, J. D., et al. (2019). Evaluating the surface chemistry of black phosphorus during ambient degradation. *Langmuir* 35 (6), 2172–2178. doi:10.1021/acs.langmuir.8b04190

Gamage, S., Fali, A., Aghamiri, N., Yang, L., Ye, P., and Abate, Y. (2017). Reliable passivation of black phosphorus by thin hybrid coating. *Nanotechnology* 28 (26), 265201. doi:10.1088/1361-6528/aa7532

García-Sancho, C., Cecilia, J., Mérida-Robles, J., González, J. S., Moreno-Tost, R., Infantes-Molina, A., et al. (2018). Effect of the treatment with H3PO4 on the catalytic activity of Nb2O5 supported on Zr-doped mesoporous silica catalyst. Case study: Glycerol dehydration. *Appl. Catal. B Environ.* 221, 158–168. doi:10.1016/j.apcatb.2017.09.016

Ge, X., Xia, Z., and Guo, S. (2019). Recent advances on black phosphorus for biomedicine and biosensing. *Adv. Funct. Mater.* 29 (29), 1900318. doi:10.1002/adfm.201900318

Guo, W., Li, J., Yang, Y., Zhang, M., Zhai, Y., Li, D., et al. (2021). Oxygen-doped carbon nitride/red phosphorus composite photocatalysts for effective visible-light-driven purification of wastewater. *Mater. Chem. Phys.* 264, 124440. doi:10.1016/j.matchemphys.2021.124440

Hanlon, D., Backes, C., Doherty, E., Cucinotta, C. S., Berner, N. C., Boland, C., et al. (2015). Liquid exfoliation of solvent-stabilized few-layer black phosphorus for applications beyond electronics. *Nat. Commun.* 6, 8563. doi:10.1038/ncomms9563

Hu, C.-X., Xiao, Q., Ren, Y.-Y., Zhao, M., Dun, G.-H., Wu, H.-R., et al. (2018). Polymer ionic liquid stabilized black phosphorus for environmental robust flexible optoelectronics. *Adv. Funct. Mater.* 28 (51), 1805311. doi:10.1002/adfm.201805311

Hu, H., Gao, H., Gao, L., Li, F., Xu, N., Long, X., et al. (2018). Covalent functionalization of black phosphorus nanoflakes by carbon free radicals for durable air and water stability. *Nanoscale* 10 (13), 5834–5839. doi:10.1039/c7nr06085h

Island, J. O., Steele, G. A., Zant, H. S. J. v. d., and Castellanos-Gomez, A. (2015). Environmental instability of few-layer black phosphorus. *2D Mater.* 2 (1), 011002. doi:10.1088/2053-1583/2/1/011002

Jia, C., Zhao, L., Cui, M., Yang, F., Cheng, G., Yang, G., et al. (2019). Surface coordination modification and electrical properties of few-layer black phosphorus exfoliated by the liquid-phase method. *J. Alloys Compd.* 799, 99–107. doi:10.1016/j.jallcom.2019.05.346

Kang, J., Wood, J., Wells, S., Lee, J.-H., Liu, X., Chen, K.-S., et al. (2015). Solvent exfoliation of electronic-grade, two-dimensional black phosphorus. *ACS Nano* 9 (4), 3596–3604. doi:10.1021/acsnano.5b01143

Kunimatsu, K., Senzaki, T., Tsushima, M., and Osawa, M. (2005). A combined surface-enhanced infrared and electrochemical kinetics study of hydrogen adsorption and evolution on a Pt electrode. *Chem. Phys. Lett.* 401 (4-6), 451–454. doi:10.1016/j.cplett.2004.11.100

Kwak, I., Im, H., Jang, D., Kim, Y. W., Park, K., Lim, Y. R., et al. (2016). CoSe2 and NiSe2 nanocrystals as superior bifunctional catalysts for electrochemical and photoelectrochemical water splitting. *ACS Appl. Mater. interfaces* 8 (8), 5327–5334. doi:10.1021/acsami.5b12093

Late, D. J. (2016). Liquid exfoliation of black phosphorus nanosheets and its application as humidity sensor. *Microporous Mesoporous Mater.* 225, 494–503. doi:10.1016/j.micromeso.2016.01.031

Lewis, E., Brent, J., Derby, B., Haigh, S. J., and Lewis, D. J. (2017). Solution processing of two-dimensional black phosphorus. *Chem. Commun.* 53 (9), 1445–1458. doi:10.1039/c6cc09658a

Li, Q., Zhou, Q., Niu, X., Zhao, Y., Chen, Q., and Wang, J. (2016). Covalent functionalization of black phosphorus from first-principles. *J. Phys. Chem. Lett.* 7 (22), 4540–4546. doi:10.1021/acs.jpclett.6b02192

Li, S., Zhang, Y., and Huang, H. (2022). Black phosphorus-based heterostructures for photocatalysis and photoelectrochemical water splitting. *J. Energy Chem.* 67, 745–779. doi:10.1016/j.jechem.2021.11.023

Li, X., and Wang, J. (2020). Phosphorus-based electrocatalysts: Black phosphorus, metal phosphides, and phosphates. *Adv. Mater. Interfaces* 7 (18), 2000676. doi:10.1002/admi.202000676

Li, X., Yoneda, M., Shimada, Y., and Matsui, Y. (2017). Effect of surfactants on the aggregation and sedimentation of zinc oxide nanomaterial in natural water matrices. *Sci. Total Environ.* 581, 649–656. doi:10.1016/j.scitotenv.2016.12.175

Liu, D., Guan, J., Jiang, J., and Tománek, D. (2016). Unusually stable helical coil allotrope of phosphorus. *Nano Lett.* 16 (12), 7865–7869. doi:10.1021/acs.nanolett.6b04128

Liu, Y., Gao, P., Zhang, T., Zhu, X., Zhang, M., Chen, M., et al. (2019). Azide passivation of black phosphorus nanosheets: Covalent functionalization affords ambient stability enhancement. *Angew. Chem.* 131 (5), 1479–1483. doi:10.1002/anie.201813218

Matthews, P. D., Hirunpinyopas, W., Lewis, E. A., Brent, J. R., McNaughter, P. D., Zeng, N., et al. (2018). Black phosphorus with near-superhydrophobic properties and long-term stability in aqueous media. *Chem. Commun.* 54 (31), 3831–3834. doi:10.1039/c8cc01789a

Miao, J., Zhang, L., and Wang, C. (2019). Black phosphorus electronic and optoelectronic devices. *2D Mater.* 6 (3), 032003. doi:10.1088/2053-1583/ab1ebd

Murthy, A., Theerthagiri, J., and Madhavan, J. (2018). Insights on Tafel constant in the analysis of hydrogen evolution reaction. *J. Phys. Chem. C* 122 (42), 23943–23949. doi:10.1021/acs.jpcc.8b07763

Oza, S., Ning, H., Ferguson, I., and Lu, N. (2014). Effect of surface treatment on thermal stability of the hemp-PLA composites: Correlation of activation energy with thermal degradation. *Compos. Part B Eng.* 67, 227–232. doi:10.1016/j.compositesb.2014.06.033

Pedersen, M. L. K., Jensen, T. R., Kucheryavskiy, S. V., and Simonsen, M. E. (2018). Investigation of surface energy, wettability and zeta potential of titanium dioxide/graphene oxide membranes. *J. Photochem. Photobiol. A Chem.* 366, 162–170. doi:10.1016/j.jphotochem.2018.07.045

Peng, L., Abbasi, N., Xiao, Y., and Xie, Z. (2020). Black phosphorus: Degradation mechanism, passivation method, and application for *in situ* tissue regeneration. *Adv. Mater. Interfaces* 7 (23), 2001538. doi:10.1002/admi.202001538

Ryder, C. R., Wood, J. D., Wells, S. A., Yang, Y., Jariwala, D., Marks, T. J., et al. (2016). Covalent functionalization and passivation of exfoliated black phosphorus via aryl diazonium chemistry. *Nat. Chem.* 8 (6), 597–602. doi:10.1038/nchem.2505

Shen, J., Liu, L., Huang, W., and Wu, K. (2021). Polyvinylpyrrolidone-assisted solvent exfoliation of black phosphorus nanosheets and electrochemical sensing of p-nitrophenol. *Anal. Chim. Acta* 1167, 338594. doi:10.1016/j.aca.2021.338594

Smith, J., Hagaman, D., and Ji, H. (2016). Growth of 2D black phosphorus film from chemical vapor deposition. *Nanotechnology* 27 (21), 215602. doi:10.1088/0957-4484/27/21/215602

Sresht, V., Padua, A., and Blankschtein, D. (2015). Liquid-phase exfoliation of phosphorene: Design rules from molecular dynamics simulations. *ACS Nano* 9 (8), 8255–8268. doi:10.1021/acsnano.5b02683

Su, S., Xu, B., Ding, J., and Yu, H. (2019). Large-yield exfoliation of few-layer black phosphorus nanosheets in liquid. *New J. Chem.* 43 (48), 19365–19371. doi:10.1039/c9nj04757c

Suryawanshi, S., More, M., and Late, D. (2016). Exfoliated 2D black phosphorus nanosheets: Field emission studies. *J. Vac. Sci. Technol. B* 34 (4), 041803. doi:10.1116/1.4945433

Tang, B., Gao, E. L., Xiong, Z. Y., Dang, B., Xu, Z. P., and Wang, X. G. (2018). Transition of graphene oxide from nanomembrane to nanoscroll mediated by organic solvent in dispersion. *Chem. Mater.* 30 (17), 5951–5960. doi:10.1021/acs.chemmater.8b02083

Tiouitchi, G., Raji, M., Mounkachi, O., Ali, M. A., Mahmoud, A., Boschini, F., et al. (2019). Black phosphorus-based polyvinylidene fluoride nanocomposites: Synthesis, processing and characterization. *Compos. Part B Eng.* 175, 107165. doi:10.1016/j.compositesb.2019.107165

van Druenen, M. (2020). Degradation of black phosphorus and strategies to enhance its ambient lifetime. *Adv. Mater. Interfaces* 7 (22), 2001102. doi:10.1002/admi.202001102

Wang, J. H., Zhang, Z. C., He, D. Y., Yang, H., Jin, D. X., Qu, J., et al. (2020). Comparative study on the adsorption capacities of the three black phosphorus-based materials for methylene blue in water. *Sustainability* 12 (20), 8335. doi:10.3390/su12208335

White, B., Banerjee, S., O'Brien, S., Turro, N. J., and Herman, I. P. (2007). Zeta-potential measurements of surfactant-wrapped individual single-walled carbon nanotubes. *J. Phys. Chem. C* 111 (37), 13684–13690. doi:10.1021/jp070853e

Wu, S., He, F., Xie, G., Bian, Z., Luo, J., and Wen, S. (2018). Black phosphorus: Degradation favors lubrication. *Nano Lett.* 18 (9), 5618–5627. doi:10.1021/acs.nanolett.8b02092

Xue, Y., Zhang, Q., Wang, W., Cao, H., Yang, Q., and Fu, L. (2017). Opening two-dimensional materials for energy conversion and storage: A concept. *Adv. Energy Mater.* 7 (19), 1602684. doi:10.1002/aenm.201602684

Yan, S., Song, H., Wan, L. F., Lin, S., Wu, H., Shi, Y., et al. (2020). Hydroxyl-Assisted phosphorene stabilization with robust device performances. *Nano Lett.* 20 (1), 81–87. doi:10.1021/acs.nanolett.9b03115

Yan, Z., He, X., She, L., Sun, J., Jiang, R., Xu, H., et al. (2018). Solvothermal-assisted liquid-phase exfoliation of large size and high quality black phosphorus. *J. Materiomics* 4 (2), 129–134. doi:10.1016/j.jmat.2018.01.003

Yao, F., Wu, Q., Lei, Y., Guo, W., and Xu, Y. (2008). Thermal decomposition kinetics of natural fibers: Activation energy with dynamic thermogravimetric analysis. *Polym. Degrad. Stab.* 93 (1), 90–98. doi:10.1016/j.polymdegradstab.2007.10.012

Yasaei, P., Behranginia, A., Foroozan, T., Asadi, M., Kim, K., Khalili-Araghi, F., et al. (2015). Stable and selective humidity sensing using stacked black phosphorus flakes. *ACS Nano* 9 (10), 9898–9905. doi:10.1021/acsnano.5b03325

Zhang, S. Y., Zhang, X. J., Lei, L., Yu, X. F., Chen, J. W., Ma, C., et al. (2019). pH-dependent degradation of layered black phosphorus: Essential role of hydroxide ions. *Angew. Chem. Int. Ed. Engl.* 58 (2), 467–471. doi:10.1002/anie.201809989

Zhang, Y., Dong, N., Tao, H., Yan, C., Huang, J., Liu, T., et al. (2017). Exfoliation of stable 2D black phosphorus for device fabrication. *Chem. Mater.* 29 (15), 6445–6456. doi:10.1021/acs.chemmater.7b01991

Zhao, W., Xue, Z., Wang, J., Jiang, J., Zhao, X., and Mu, T. (2015). Large-scale, highly efficient, and green liquid-exfoliation of black phosphorus in ionic liquids. *ACS Appl. Mater. interfaces* 7 (50), 27608–27612. doi:10.1021/acsami.5b10734

Zhou, Q., Chen, Q., Tong, Y., and Wang, J. (2016). Light-induced ambient degradation of few-layer black phosphorus: Mechanism and protection. *Angew. Chem. Int. Ed.* 55 (38), 11609–11613. doi:10.1002/ange.201605168